Received: 28 August 2022 | Revised: 2 December 2022 | Accepted: 22 December 2022

DOI: 10.1002/esp.5528

RESEARCH ARTICLE

ESPL WILEY

Near-surface temperatures and potential for frost weathering in blockfields in Norway and Svalbard

Maria Peter[1] | Jane Lund Andersen[2] | Francis Chantel Nixon[1] | Bernd Etzelmüller[3] | Sebastian Westermann[3] | Ola Fredin[4]

[1]Department of Geography, Norwegian University of Science and Technology, Trondheim, Norway

[2]Department of Geoscience, Aarhus University, Aarhus, Denmark

[3]Department of Geosciences, University of Oslo, Oslo, Norway

[4]Department of Geoscience and Petroleum, Norwegian University of Science and Technology, Trondheim, Norway

Correspondence
Maria Peter, Department of Geography, Norwegian University of Science and Technology, NO-7491 Trondheim, Norway.
Email: maria.peter@ntnu.no

Funding information
Norges Forskningsråd, Grant/Award Number: ES676559

Abstract

Blockfields remain enigmatic regarding their origin, internal structure, surface processes, and glaciological implications. In Scandinavia, blockfields are found on high-elevation, low-relief mountains (plateaus) across the Arctic and Subarctic. In this study, we present a 1D numerical model that uses near-surface temperatures measured between summer 2018 and summer 2020 to calculate frost-cracking intensities (FCI) within the ground column in three different blockfields in Norway and Svalbard. Eighty-nine miniature temperature loggers were distributed on Tron Mountain (1650 m a.s.l.) in Alvdal, Gamlemsveten (780 m a.s.l.) near Ålesund in southwestern Norway and on Platåberget (460 m a.s.l.) near Longyearbyen, Svalbard. We modelled FCI by scaling the time spent in the frost cracking window (between −3 and −8°C) with the temperature gradient and a penalty function for distance to available water. At Tron and Gamlemsveten, ground temperatures never reached the frost cracking window at one third of our sites due to insulation by a thick snow cover in depressions and on the lee sides of summits. The highest FCI (0.05–0.4 K m) are obtained where the subsurface consists of boulders and stones in a matrix of relatively fine sediment (sand, silt, gravel). In contrast, very low FCI (0.003–0.02 K m) were modelled for blocky layers with large air-filled pores because of the low water availability. On Platåberget, all sensors reached the frost-cracking window during the annual temperature cycle, but FCI are extremely low (0.0004–0.15 K m) as water availability is limited due to (i) permafrost and (ii) near-surface temperatures remaining below the frost-cracking window for 3/4 of the year. This indicates that boulder-rich blockfields with air-filled hollows are preserved in very cold climates, whereas warmer, maritime settings with higher availability of fine interstitial material place blockfields in the fast lane for frost weathering.

KEYWORDS
blockfields, frost-cracking, landscape evolution, periglacial erosion, thermal modelling

1 | INTRODUCTION

Blockfields are found across the Arctic and Subarctic, usually covering high-elevation, low-relief mountains (plateaus). They often exhibit a stratigraphy with boulders and cobbles with large, air-filled pore spaces which gradually transitions into a finer-grained layer that in turn overlies bedrock (Goodfellow, 2012; Goodfellow et al., 2009). Ballantyne (1998), who uses the term 'mountain-top detritus' in the sense that we here use blockfield, classifies blockfields into three categories: (1) the classic 'blockfield', which is a layer of coarse clasts with air-filled voids at the top and increasingly fine-grained infill towards the bottom; (2) the sandy-diamict type, where clasts of different sizes sit in a sandy matrix; and (3), the silt-rich diamicts, where clasts sit in a silty matrix of frost-susceptible fines, with signs of frost sorting present,

and the coarsest clasts are often concentrated in the uppermost layer. There is an active debate concerning the genesis and age of the blockfield landform, with no established consensus regarding palaeoglaciological implications and present-day activeness of the landform (e.g., Ballantyne, 2010; Egholm et al., 2015; Goodfellow et al., 2014).

In southern Norway, Nesje et al. (1988) observed that the lowermost limits of blockfields rise from ~500 m a.s.l. at the outermost coast of Møre and Romsdal county to ~1500 m a.s.l. further inland. They correlate this gradient with the increasing surface elevation of the late Weichselian Fennoscandian Ice Sheet. Based on this observation, they suggest that blockfields in Norway were located in areas that remained ice free during at least parts of the Weichselian glaciation—for example, on high-lying summits protruding as nunataks (e.g., Nesje et al., 1987). Studies on rock surface weathering of blockfields in southern Norway were also interpreted to support the hypothesis of ice-free conditions (Nesje et al., 1994) as well as the apparent absence of glacial striations or glacial landforms on these blockfields (Nesje et al., 1988). For the same reasons, the lower limit of blockfields in Irish mountains was also interpreted as a reflection of the maximum vertical level of the ice sheet, with blockfield summits having existed as palaeo-nunataks (Rae et al., 2004; Warren, 1979). Also in the Tatra Mountains in Slovakia and Poland, blockfields have been interpreted as features above the glaciation limit (Zasadni & Kłapyta, 2014).

A competing hypothesis of Scandinavian blockfield origin was put forward by Sollid and Sørbel (1979) and later by Kleman (1994), suggesting that blockfields and other landforms can survive below cold-based parts of ice sheets. According to this hypothesis, the Scandinavian blockfields indicate areas of cold-based ice of the Fennoscandian Ice Sheet during at least the last glacial period (c. 35,000–10,000 years ago) (Fjellanger et al., 2006; Kleman & Stroeven, 1997; Rea et al., 1996; Strømsøe & Paasche, 2011). The suggestion of blockfield survival beneath cold-based ice also requires that the blockfields pre-date at least the last glaciation. Numerical landscape evolution modelling has shown that regolith-covered low-relief summits can develop by glacial and periglacial erosion over multiple glacial cycles (Anderson, 2002; Egholm et al., 2015, 2017). These studies also indicate that cold-based, low-erosive conditions gradually develop on the high plateaus as a function of gradual relief reduction and smoothing of the plateau regions combined with increased incision of (and ice flow through) adjacent glacial valleys (Egholm et al., 2015, 2017, Kessler et al., 2008).

If blockfields have indeed persisted through several glaciations, this raises the question of how and when they were initially formed. Several studies have attempted to constrain the age of blockfields by inferring erosion rates from cosmogenic nuclide chronometry (Andersen et al., 2018; Briner et al., 2006; Fjellanger et al., 2006; Goehring et al., 2008; Goodfellow et al., 2014; Jansen et al., 2019; Marquette et al., 2004; Skov et al., 2020). These studies show that material from plateau blockfield areas generally yields older ages (higher cosmogenic nuclide concentrations) than adjacent glacially scoured valley and slope areas. In most cases, the higher cosmogenic nuclide concentrations are interpreted to indicate minimally erosive ice during the last glacial period. Interpreting cosmogenic nuclide data from blockfield depth profiles to infer erosion rates can be complicated, because of possible past or present mixing processes in the ground column—that is, frost heave and cryoturbation, as well as complex exposure histories with multiple periods of exposure (and mixing) interspersed with periods of (cold-based) ice cover (Andersen et al., 2018). Although inversion modelling of cosmogenic nuclide data can help to constrain the near-surface residence times and mixing rates of blockfield materials (Andersen et al., 2018), cosmogenic nuclide data cannot fully reveal the genesis of the blockfield landform.

The discovery of clay minerals, such as kaolinite and gibbsite in blockfields in Norway (Roaldset et al., 1982), may indicate that the blockfields pre-date the cold Quaternary period, as these clay minerals are often assumed to form in temperate or warmer climatic settings (Marquette et al., 2004; Staiger et al., 2005; Strømsøe & Paasche, 2011). This interpretation implies extremely low blockfield weathering, creep and erosion rates (including any glacial erosion), despite exposure to subaerial weathering at least during ice-free intervals. Others have stated that clay minerals might also form in colder climate settings in blockfields, conditioned by favourable moisture and pH conditions (Goodfellow, 2012; Hall et al., 2002; Pope et al., 1995). In that case the presence of clay minerals is not indicative of old, slowly weathering blockfields.

Blockfields are a feature of periglacial and cryo-conditioned landscapes. Their unique stratigraphy affects the local microclimate, by lowering ground temperatures in comparison to adjacent areas without blockfield cover (Berthling & Etzelmüller, 2011; Lilleøren et al., 2012). Temperature profiles from blockfields in eastern Norway show anomalies of −1.3 to −2.0°C compared to surrounding till and bedrock areas (Juliussen & Humlum, 2008). Among other processes such as thermal cracking or pressure release fracturing from glacial unloading, frost cracking is likely to be one of the main mechanical weathering processes on Scandinavian high-elevation plateaus in the present-day climate (Fraser, 1959; Hall et al., 2002). Andersen et al. (2018) found that blockfields in the high plateau area of Reinheimen, Norway, show relatively low erosion rates (~4–8 m/Myr). Similarly, Granger et al. (2001) document that boulder armoured slopes in the Rocky Mountains erode much slower than surrounding soil-covered areas. Still, there exist knowledge gaps about the intensity of (frost)-weathering mechanisms presently or formerly active in blockfields and regarding the role of permafrost.

Hales and Roering (2007) developed a simple model for frost cracking, which relies on ground temperature and water availability as input. This was further developed by Andersen et al. (2015) and Egholm et al. (2015) to simulate frost-cracking rates. In this study we apply the frost-cracking model of Andersen et al. (2015) to measured ground temperatures and idealized stratigraphies in three different blockfields located along a climatic gradient from permafrost-free and marginal permafrost locations in southern Norway to a continuous permafrost site on Svalbard. This allows us to drive the model with realistic ground surface temperatures and analyse the effects of ground stratigraphy on frost-cracking intensity (FCI), including the impact of seasonal snow cover. We use these results to discuss two hypotheses: (1) blockfields are 'old' landforms which were preserved under a cold-based ice cover, or on nunataks, during one or several glacial cycles; (2) blockfields are a post-glacial, 'young', landform which formed after the last deglaciation.

2 | STUDY SITES

Three field sites were chosen with the goal of investigating blockfields in different climates (Figure 1): Tron (continental site with marginal permafrost), Gamlemsveten (maritime site with no permafrost), and

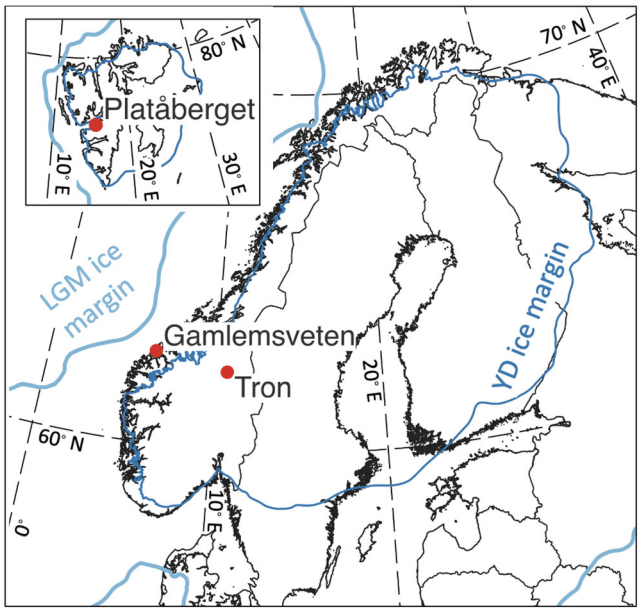

FIGURE 1 Overview of the three field sites. LGM (Last Glacial Maximum) and YD (Younger Dryas) ice sheet extent outline from Hughes et al. (2016). [Color figure can be viewed at wileyonlinelibrary.com]

Platåberget (cold permafrost and low precipitation). In the following, each of these sites is presented with a focus on climate, blockfield characteristics, permafrost and the timing of last deglaciation. For each site, we obtain consistent air temperature and precipitation information for the normal period (1961–1990) and the 1-year study periods by using measurements from the closest-lying climate station which has data available for both periods (obtained from seklima.met.no). These stations are Vigra (22 m a.s.l., 26 km west of Gamlemsveten), Røros (55 km NE of Tron, 625 m a.s.l.) and Longyearbyen/Svalbard Lufthavn (28 m a.s.l.) at the foot of Platåberget. Air temperatures were scaled to the altitude of the blockfield sites by using a wet lapse rate of 0.5°C/100 m, while precipitation was increased by 10% per 100 m below 1000 m a.s.l. and 5% for elevations above 1000 m a.s.l. (following Jansson et al., 2007). For Tron and Platåberget, air temperature measurements at the blockfield sites are available for the study period (Table 1), which allows estimating the accuracy of the altitudinal scaling to around 0.2 (Tron) to 0.7°C (Platåberget).

2.1 | Tron Mountain

The Tron Mountain blockfield (~1650 m a.s.l.)is located in East Norway (Figures 1 and 2). The climate of the blockfield is classified as Polar Tundra (ET) after Koeppen–Geiger (Geiger, 1954; Peel et al., 2007) with a mean air temperature (MAT) of −2.7°C (weather station at summit borehole, study period, unpublished data, University of Oslo) and mean annual precipitation (MAP) of 1020 mm (study period, Table 1).

The blockfield is characterized by very angular gabbro clasts spanning a large size range (0.05–3.5 m in diameter), with some sandy patches with sorted ground. Thin algae and lichen vegetation exists mostly on top of fine sediment and on the rocks (Figure 3). Permafrost of around −0.5°C is present today at the summit area with an active layer thickness between 12 and 15 m (measurements from summit borehole, see Figure 2). The last Fennoscandian Ice Sheet retreated from this area at ~10 ka (Hughes et al.2016, Stroeven et al., 2016).

2.2 | Gamlemsveten

Gamlemsveten (~800 m a.s.l.) is situated on the west coast of Norway, and experiences a temperate, maritime climate (Koeppen classification Dfc) with cold summers, no dry season, and mild winters (i.e., wet snow and rain). The MAT of the Gamlemsveten blockfield site during the study period was 3.9°C (Table 1), while the mean air temperature in January was −1.6°C and in August 10.6°C (calculated as for annual averages). The calculated mean precipitation was around 3900 mm (Table 1). The surficial geology of the Gamlemsveten blockfield includes medium-large clasts (typically 0.2–1.20 m) of hornblende-rich migmatite gneiss, which are slightly rounded to rounded. Large areas are covered in thick vegetation (mainly crowberry, some graminoids, moss and lichen) on top of fine sediment with initial soil development, while in some areas the blocks themselves are covered with 2–3 cm of mosses and lichens (Figures 4 and 5, left and middle pictures). Sorted ground indicates present or past freeze–thaw processes, but no permafrost exists today (derived from this study's surface temperature measurements and ground temperature modelling). The Fennoscandian Ice Sheet retreated from Gamlemsveten ~14–15 ka and the mountain has remained ice free since then (Hughes et al., 2016; Roaldset et al., 1982; Stroeven et al., 2016).

2.3 | Platåberget

Platåberget (also known as Platåfjellet) is a plateau mountain situated 1 km west of the Longyearbyen settlement on the Svalbard archipelago (Figure 1). The study area of Platåberget occupies elevations between 440 and 475 m a.s.l. (Figure 6). MAP is very low in this area with ~300–350 mm, and the mean temperature during the study period was −5.4°C according to Platåberget weather station (SN99843; seklima.met.no). We measured a mean snow depth at the ground surface temperature measurement sites of 66 cm with variations from 20 to 130 cm throughout May 2019. The blockfield on Platåberget is characterized by sandstone clasts, ranging from pebbles to blocks of 1 m in diameter. The site has a large variety of surface forms, ranging from blockfield morphology with unsorted large angular blocks to fine-grained patches with rounded pebbles, sorted circles and water track areas where moss covers the finer sediment (Figure 7). Lønne (2017) also identified areas with meltwater channels from the last deglaciation in the lower and more inclined part of the blockfield at the northeast end.

Platåberget blockfield is underlain by continuous permafrost, which has a depth of around 500 m and around −6°C (Isaksen et al., 2001) at the ZAAT (zero annual amplitude temperature, measured at the depth where the influence of seasonal temperature fluctuations ceases; Biskaborn et al., 2019). The active layer measured during excavation varied between 50 and 70 cm depth (end of August and beginning of September), depending on the surface material and stratigraphy (fine-grained sorted ground or openwork blockfield), while the modelled maximum active layer varied between 0.9 and

TABLE 1 Overview of climatic parameters and elevation at all sites.

Site	MAT normal period (°C)	MAT study period (°C)	MAP normal period (mm)	MAP study period (mm)	Elevation above sea level (m)
Tron	(−4.9)	−2.7 (−2.9)	(985)	(1020)	1650
Gamlems-veten	(2.9)	(3.9)	(2805)	(3886)	800
Platåberget	(−8.4)	−5.4 (−4.7)	(295)	(355)	440

Note: MAT, mean air temperature; MAP, mean annual precipitation. Numbers without parentheses refer to measurements at the site (near summit borehole for Tron, Figure 2; 5 km west of blockfield at similar elevation for Platåberget, Figure 6). Numbers in parentheses refer to values obtained by elevation scaling from the closest weather station with continuous record (Røros for Tron, Vigra for Gamlemsveten, Svalbard Lufthavn/Longyearbyen for Platåberget, seklima.met.no). See text, Section 2.

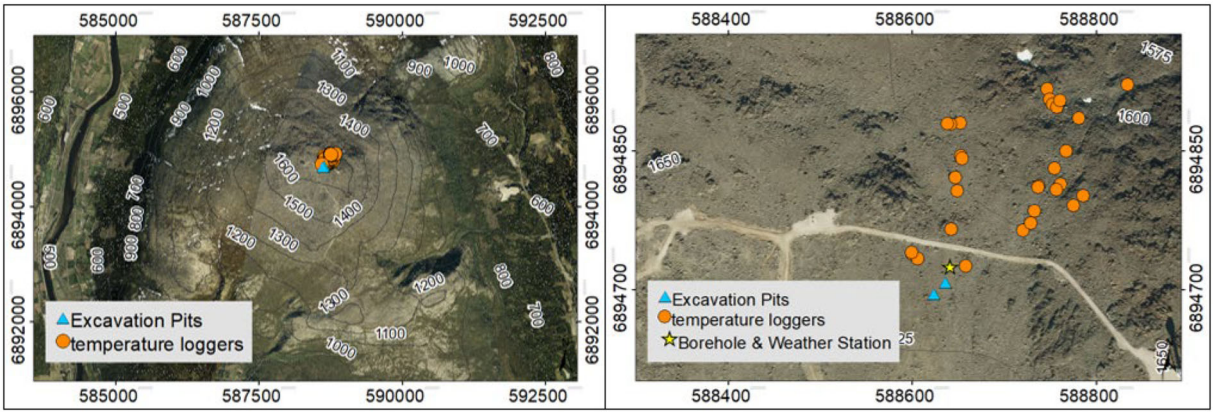

FIGURE 2 Left: overview map of Tron Mountain in Østerdalen. Right: detail map of the summit blockfield with temperature logger distribution and location of excavation pits, borehole and weather station. [Color figure can be viewed at wileyonlinelibrary.com]

FIGURE 3 Tron blockfield, left and middle: the orange DGPS antenna is about 50 cm high. Right: profile of one of the excavation pits. Layer I describes a sand-rich layer in the uppermost 50 cm; layer II is a gravel-rich layer reaching from 50 cm depth until the bottom of the profile. The circle indicates the location of a cobble-shaped clast, and the brown hatched area indicates a brownish layer, probably associated with Fe oxidation. [Color figure can be viewed at wileyonlinelibrary.com]

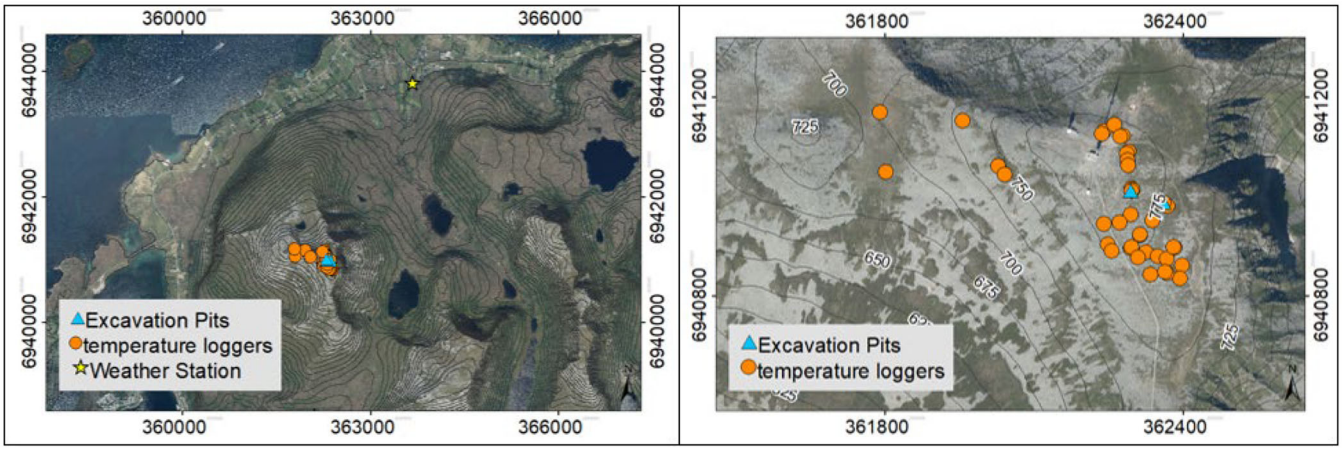

FIGURE 4 Left: overview of Gamlemsveten Mountain with the Hildreelv weather station north of the massif. Right: distribution of temperature sensors and excavation pits at the summit. [Color figure can be viewed at wileyonlinelibrary.com]

FIGURE 5 Left and middle: pictures of Gamlemsveten blockfield. The DGPS pole in the middle is about 1.50 m tall. Right: profile of excavation pit 2, where layer I describes 60% subangular cobbles and boulders and pores filled with air and some organic material, covered by a 4–9 cm thick layer of dead and alive plant material (mainly moss and heath). Layer II is a transition zone with 50% clasts (cobbles and boulders, subangular to subrounded) and pores filled with sand, fine gravel and humous material. Layer III is a yellow-brown matrix-supported layer with around 40% subrounded boulders and cobbles, silty sand and some gravel. [Color figure can be viewed at wileyonlinelibrary.com]

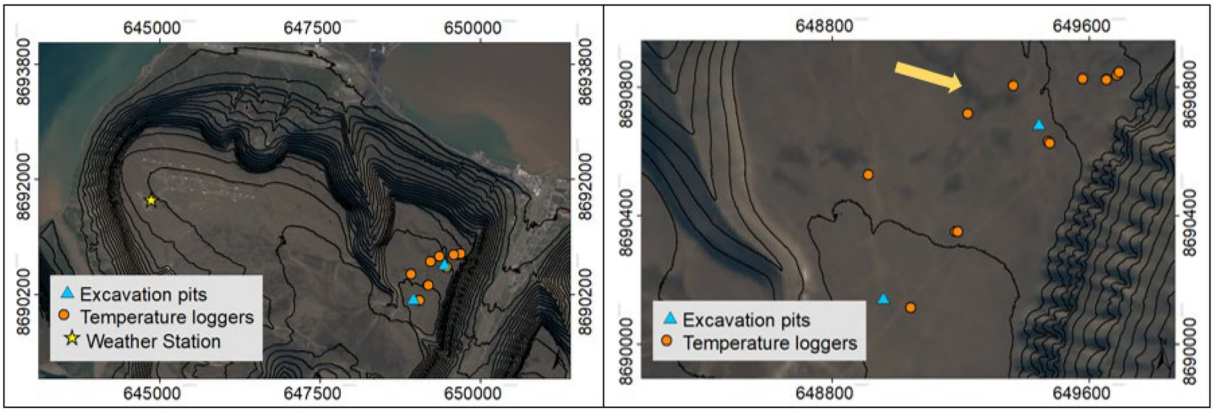

FIGURE 6 Location of the weather station, temperature loggers and excavation pits on Platåberget. The yellow arrow indicates an area with sorted stripes, as shown in Figure 7. [Color figure can be viewed at wileyonlinelibrary.com]

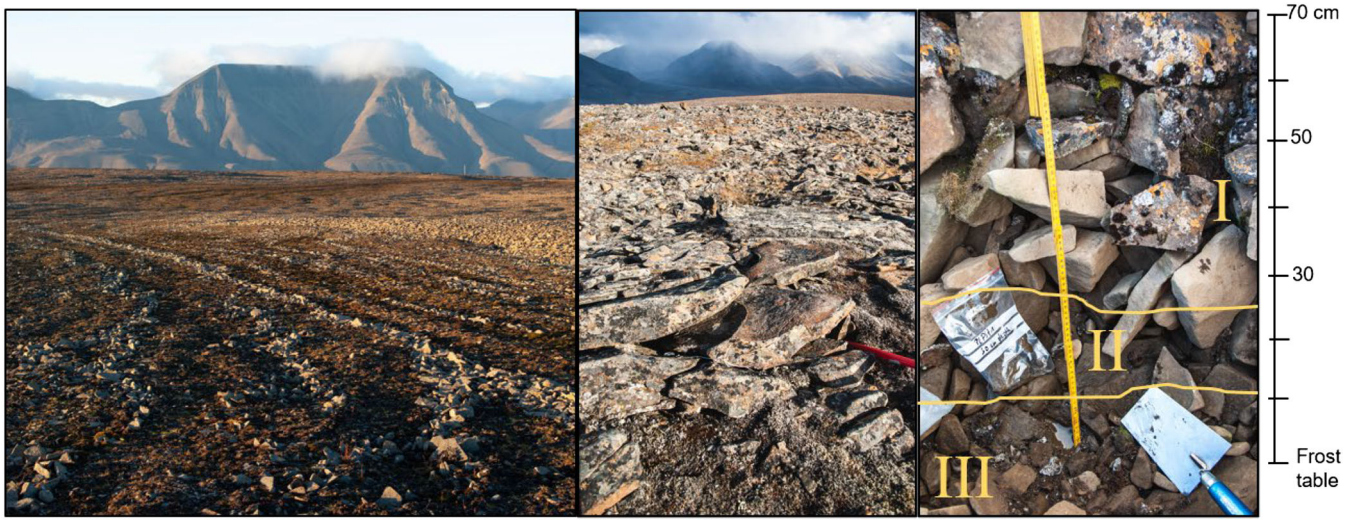

FIGURE 7 Platåberget. Left: area with sorted stripes, fine material and small rocks; location indicated in right-hand map of Figure 6. Middle: angular blocks and air-filled hollows at points 2 and 3. Right: pit 1, 70 cm deep, water-saturated layer above frost table (III), medium large (5–30 cm in diameter) angular blocks and air-filled hollows (I), 50% filled with silt, sand and gravel in lower parts of the pit (II). [Color figure can be viewed at wileyonlinelibrary.com]

1.4 m (for matrix-supported and air-filled, clast-supported stratigraphy, respectively). Platåberget was deglaciated between 12 and 11 ka, according to Hughes et al. (2016).

3 | METHODS

First, we provide an overview of in situ measurements and the observed blockfield stratigraphies. Thereafter, the idealized blockfield stratigraphies used as input for the ground temperature modelling are presented, and lastly modelling of the ground temperature field and FCI is explained.

3.1 | In situ measurements

Miniature temperature sensors (DS1922L by Maxim Integrated), also called iButtons, were placed in a large variety of settings in all three blockfields. The settings range from depth profiles of two to three sensors emplaced in fine-grained sediment or into hollows between blocks (down to 1.20 m below the surface) to single sensors next to large boulders or situated in hollow spaces between blocks, and from non-vegetated sites to sites with thick moss cover. The loggers were distributed to cover the range of morphology and surface characteristics of each blockfield. Additionally, the sensors cover differences in lithologies (sand- and mudstone for Platåfjellet, gabbro on Tron, gneiss on Gamlemsveten) and elevation above sea level (400–1650 m a.s.l.), as well as climate (mean annual air temperature [MAAT]: −5.4 to 3.9°C, MAP: 355–3900 mm; Table 1).

The logger resolution was set to 0.0625°C and the measurement interval to 3 h. The length of the survey was 2 years at Tron and Platåberget, and 1 year at Gamlemsveten, though only 1 year of data is used for all the sites. Snow depth was measured with differential GPS precision at each logger site at the peak of snow depth (end of March at Gamlemsveten and Tron, end of April/May on Svalbard). Snow depths were measured in a grid of 5 points, with the first measurement at exactly the logger position and the other four in a 1 m spacing apart from the central position into each geographic direction, to capture the variability of snow cover at each site. Snow density measurements were performed each year at two to three locations/snow pits per blockfield site.

At each blockfield site at least two deeper excavations were made to relate surface forms to subsurface stratigraphies (see Figures 2, 4 and 6 for locations). From those manually excavated pits we logged the local stratigraphy with regard to grain sizes, porosity, water/ice and minerogenic/organic content, as well as the coarse fraction of blocks and rocks. This is needed to model the temperature field below each logger. The sites generally fall into two categories: first, an openwork blockfield or 'air-filled, clast supported' stratigraphy (Table 2); and, second a matrix-supported stratigraphy (Table 3). For each of the 89 logger sites the stratigraphy was estimated and documented while deploying the dataloggers.

The 'openwork blockfield type' features larger blocks and rocks with a high air-filled porosity down to 1.5 m depth, followed by finer material and stones between 1.5 and 2 m and from 2 to 10 m water-saturated bedrock with a porosity of 3%, which is in the range of values assumed by Myhra et al. (2017, 2019) for bedrock in the Norwegian mountains (Table 1). The 'matrix-supported stratigraphy' type features fine (silt, sand, gravel) sediment and some rocks from 0 to 0.2 m depth, saturated gravel, sand, and clasts from 0.2 to 2 m, and below 2 m again saturated bedrock with a 3% porosity (Table 2). For all simulations, the soil freezing characteristic for sand is employed (Westermann et al., 2013).

3.2 | Simulations of ground temperature profiles

The field measurements of ground surface temperature were used to force the ground thermal model CryoGrid 2 (Westermann et al., 2013) to simulate temperature profiles for the two idealized subsurface stratigraphies. For these stratigraphies, time- and depth-resolved fields of ground temperatures, as well as water and ice contents, were simulated at each logger site, which was subsequently used as input for evaluations of the FCI (Section 3.3).

CryoGrid 2 is a simple heat conduction model which numerically solves the heat conduction equation:

$$c_{\text{eff}}(z,T)\frac{\partial T}{\partial t}-\frac{\partial}{\partial z}\left[k(z,T)\frac{\partial T}{\partial z}\right]=0, \quad (1)$$

with t denoting time (s), T temperature (K), z the depth below the surface (m) and k the thermal conductivity ($Wm^{-1}\,K^{-1}$). The effective

TABLE 2 Air-filled, clast-supported stratigraphy.

Depth (m)	Volume of water/ice content	Volume of mineral content	Description (mineral soil type sand is assumed)
0–1.5	0.01	0.55	Blocky layer, air-filled voids
1.5–2.0	0.15	0.75	Unsaturated unconsolidated layer
2.0–10	0.03	0.97	Saturated bedrock layer

TABLE 3 Matrix-supported stratigraphy.

Depth (m)	Volume of water/ice content	Volume of mineral content	Description (mineral soil type sand is assumed)
0–0.2	0.25	0.7	Blocky layer, voids filled with gravel and sand
0.2–2.0	0.3	0.7	Saturated unconsolidated layer
2.0–10	0.03	0.97	Saturated bedrock layer

volumetric heat capacity c_{eff} (J m^{-3} K^{-1}) accounts for the latent heat of freezing/melting of soil water/ice as

$$c_{eff} = c(z,T) + L\frac{\partial \theta_w}{\partial T}. \quad (2)$$

Here, the first c term represents the 'normal' heat capacity of the soil material, which is calculated from the volumetric fractions of mineral, water and ice (Westermann et al., 2013). The second term represents latent heat effects, with $L = 334$ MJ m^{-3} denoting the specific volumetric latent heat of fusion of water, and $\partial\theta_w/\partial T$ the soil freezing characteristic, which determines the unfrozen water content for temperatures below the freezing point of free water. $\partial\theta_w/\partial T$ depends on the soil type, and the parametrization of Dall'Amico et al. (2011) is used in the model. While CryoGrid 2 accounts for the phase change of soil water and ice, the sum of water and ice contents is assumed constant; that is, changes in water content due to precipitation and evaporation are not accounted for. The temperature-dependent thermal conductivity is calculated from the volumetric fractions of the soil constituents mineral, air, water and ice, following the parametrization of Cosenza et al. (2003). A detailed description of CryoGrid 2 is provided in Westermann et al. (2013).

In this study, the temperature forcing at the upper boundary was provided by the field measurements, and the snow depth was set to zero as the measurements provide temperatures below the seasonal snow cover.

For model initialization, we first assign a steady-state temperature profile with the average annual temperature of the measurements at the surface and a geothermal heat flux of 50 mW m^{-2}. Secondly, the model forcing is looped for a number of years until the simulated daily average temperatures in the uppermost 5 m are stable within 0.01°C from one to the next annual run.

Figure 8 displays an example simulation with the matrix-supported stratigraphy for a site on Tron blockfield characterized by a thick snow cover. During spring, ground surface temperatures are confined to 0°C for almost 2 months due to the melting snow cover, while ground temperatures at 1 m depth remain at the freezing point until February, as the thick snow cover prevents a fast cooling of the ground. The measurements and simulations suggest that frost cracking only occurs near the surface, as ground temperatures at 0.5 and 1.0 m depth are always warmer than −3°C and thus never reach the frost-cracking window (FCW; Section 3.3).

3.3 | Modelling of FCI

Following Anderson (1998), Hallet et al. (1991) and Walder and Hallet (1985) (Equations 3 and 4), we assume that frost cracking occurs by ice segregation when temperatures in the subsurface are within the FCW (−3 to −8°C).

We calculate the FCI as a semi-quantitative measure that takes three aspects into account: (1) subsurface temperatures within the FCW; (2) the vertical temperature gradient (dT/dz); and (3) a term representing the availability of liquid water for segregation ice formation, as defined in Andersen et al. (2015):

$$\mathrm{FCI}(z,T) = \begin{cases} \left|\frac{dT}{dz}\right| V_w(z) & \text{if } -8^\circ\mathrm{C} < T < -3^\circ\mathrm{C} \\ 0 & \text{else,} \end{cases} \quad (3)$$

where z denotes depth, t time and T temperature. $V_w(z)$ defines the water volume available for ice segregation:

$$V_w(z) = \int_l \phi(z') w_f(z') e^{-\Gamma(z')} dz'. \quad (4)$$

where ϕ is the porosity, w_f is the water fraction (as simulated by CryoGrid 2, Section 3.2) and $e^{-\Gamma(z')}$ is a penalty function which depends on the distance the water travels across a path length (l) to the freezing front and the flow resistance.

4 | RESULTS

4.1 | Temperature measurements

In the Tron blockfield (Figure 9, upper panel), we observed a significant variability of surface temperatures during winter, depending on snow cover and settings of sensors (iButtons) within the blockfield (mean: 0.6°C; winter temperature range: 9.7 K; winter mean: −2.15°C; winter standard deviation: 1.35 K; winter period defined as 01 November to 15 April). Measurement sites covered by deep snow remained relatively warm (above the FCW) and experienced only minor temperature fluctuations (range: 5 K). Sites with shallow snow cover followed air temperatures measured at the summit weather station more closely, with low temperatures of −12°C and warm spells in

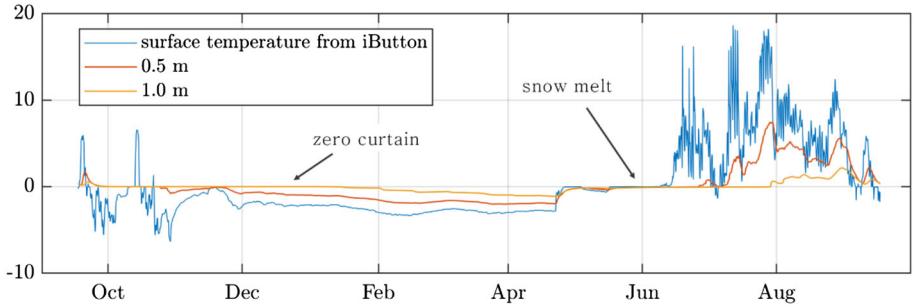

FIGURE 8 Example of temperature modelling at 0.5 m and 1 m depth forced by measured near-surface temperatures and a matrix-supported stratigraphy, showing a long zero-curtain period at 1 m depth and snow melt occurring throughout May and June. The near-surface temperature data are from a logger (iButton) at Tron blockfield. At this site, we measured a maximum snow cover of 2.40 m during the measurement period 2018/2019. [Color figure can be viewed at wileyonlinelibrary.com]

spring. Those sites were more often within the FCW throughout the season. During summer, the spatial variability of iButton temperatures is lower than in winter—only sensors placed within hollows and deeper in between the very porous stratigraphy with large boulders stayed cooler. During fall, we observe temperatures both within and outside of the FCW for all sensors, which potentially leads to strong frost cracking before the onset of snow cover and still relatively high availabilities of water.

In the Gamlemsveten blockfield (Figure 9 middle panel), we measured relatively warm near-surface temperatures (mean = 3.4°C) with medium-high variability during winter (winter mean: −0.6°C; range: 20.7 K; standard deviation: 1.46 K, for all sensors). This coastal mountain often receives warm and moist air masses during winter, which make air temperatures fluctuate above and below 0°C multiple times during the winter season. This repeatedly provides liquid water for refreezing in the rock fractures, causes freeze–thaw cycling, and pulls temperatures in and out of the FCW (in total, 23 times for the season 2019/2020). A cold spell in fall occurred when the snow cover was only thin, leading to very cold temperatures (−12°C). In summer, the spatial distribution of surface temperatures in the blockfield is largely uniform and temperatures respond almost directly to air temperatures and solar radiation. A few sensors receive direct solar radiation in summer and show unrealistically high temperatures, but winter temperatures are not affected, and they are thus retained for the analysis of frost cracking.

For the Platåberget blockfield (Figure 9, lower panel) located on Svalbard, iButton temperatures are generally much colder in winter (mean: −5°C; winter mean: −10.3°C; winter temperature range: 27.8 K; winter temperature standard deviation: 4.4 K) due to shallow snow cover and colder air temperatures. Here, we observe near-surface temperatures as low as −28°C. This is most pronounced for loggers 2, 3 and 7, which were placed in exposed positions and were often exposed to air temperatures. Logger 1 was placed within a snow patch which establishes early in fall and remains long into summer. We observe temperatures generally below the FCW during winter and some fluctuations into the window in fall and spring. The spatial distribution of near-surface temperatures is relatively uniform during spring and the snow melt phase (middle of April until middle of June), as well as in summer. Here again, fall is the most effective frost-cracking period of the year, when shallow snow cover, temperature fluctuations and relatively high amounts of water in the ground provide a high frost-cracking potential. It is important to consider the effect of permafrost at Platåberget, as two-sided freezing during fall rapidly minimizes the available water in the ground and therefore reduces the potential for frost cracking significantly (see Section 3.3).

4.2 | Snow cover

The snow cover was measured at each logger site and used to interpret the modelled data, but is not used in the model forcing itself (snow depth in the model is set to zero as the temperature sensors measured below snow cover). The average snow cover thickness at the Tron study site was 107 cm in season 2018/2019, but varied between 20 and >300 cm. At Gamlemsveten, snow cover thickness at the temperature logger points varied from 0 to 100 cm, with an average value of 30 cm for the winter season 2019/2020. In this season, the snow cover melted away and built up several times at the blockfield site, due to temperature fluctuations and rain events. At Platåberget, we measured a mean snow depth at the ground surface temperature measurement sites of 66 cm with variations from 20 to 130 cm throughout May 2019.

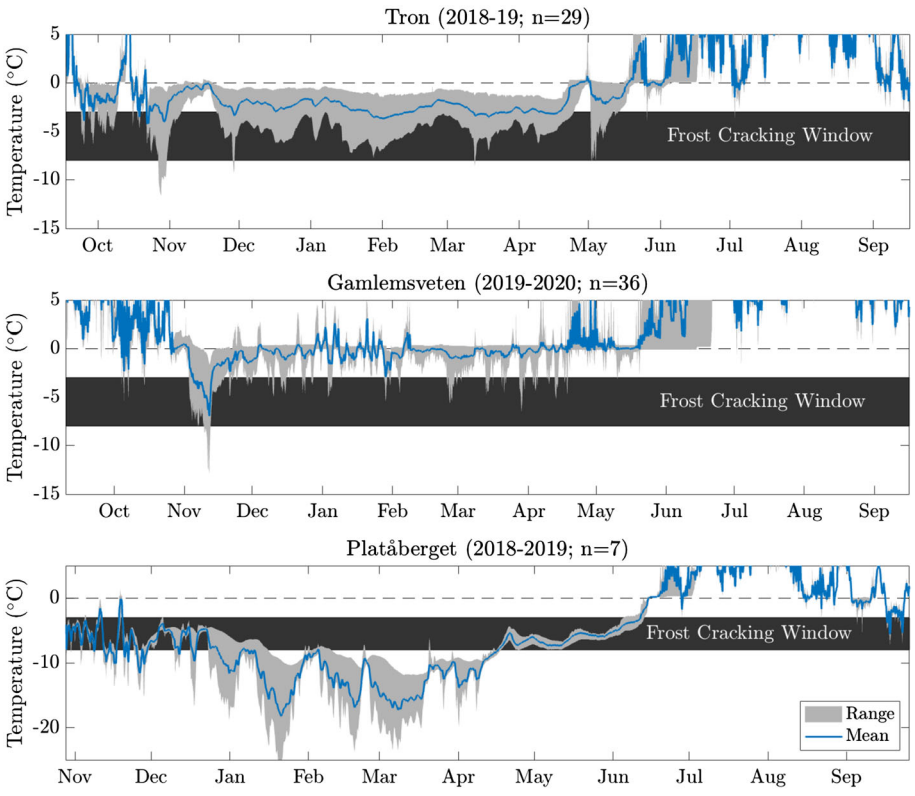

FIGURE 9 Mean and range of ground surface temperatures in all three field sites. Note the different scales of both *y*- and *x*-axes in each panel. [Color figure can be viewed at wileyonlinelibrary.com]

4.3 | Frost-cracking window

At each field site, measured near-surface temperatures reached the FCW for at least some of the logger sites (Figure 9). For the Tron blockfield, ~20% of the loggers experienced 10–20 days within the FCW, while the remaining ~80% show a high variability distributed from 20 to 170 days in the FCW (Figure 10). For the Gamlemsveten blockfield, ~50% of the loggers are in the FCW for 0–10 days, ~40% spend 10–20 days within the FCW and ~10% spend 20–35 days per year in the FCW (Figure 9). At the Platåberget blockfield, all loggers are in the FCW between 100 and 150 days per year (Figure 10), and the highest number of days in the FCW were recorded at sites with deep snow cover. In general, all sites display a strong spatial variability at scales of hundreds of metres, while Tron in particular showed strong differences in the number of days spent in the FCW.

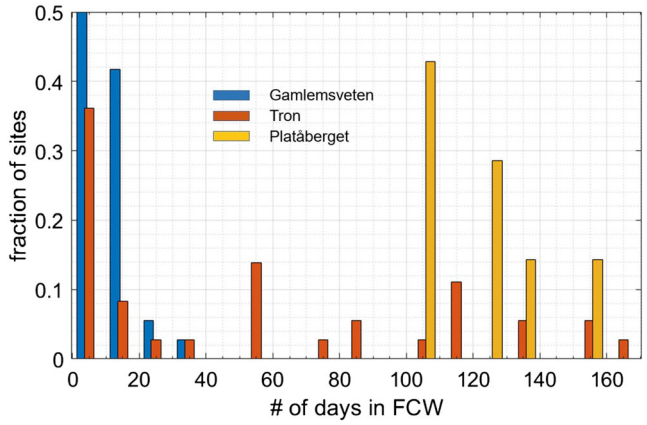

FIGURE 10 Fraction of logger sites at Tron (red), Gamlemsveten (blue) and Platåberget (yellow) where near-surface temperatures experience a certain number of days (*x*-axis) within the frost-cracking window (FCW). [Color figure can be viewed at wileyonlinelibrary.com]

4.4 | Frost-cracking intensities

FCI for all three blockfield sites were modelled from simulated temperature fields below each individual logger, using measured temperatures as the upper boundary condition. The temperature fields depend strongly on the employed stratigraphies. In Figure 11 we show the influence of stratigraphy on the temperature field at one temperature logger per blockfield site. In the left panels, the temperature field below each logger is modelled for an air-filled, clast-supported stratigraphy (see Table 2). In this stratigraphic setting, cold temperatures generally penetrate deeper into the ground than when modelled for the matrix-supported stratigraphy (Table 3). For example, at the Tron blockfield the 0°C isoline reaches 2.5 m depth (exceeds data frame), as

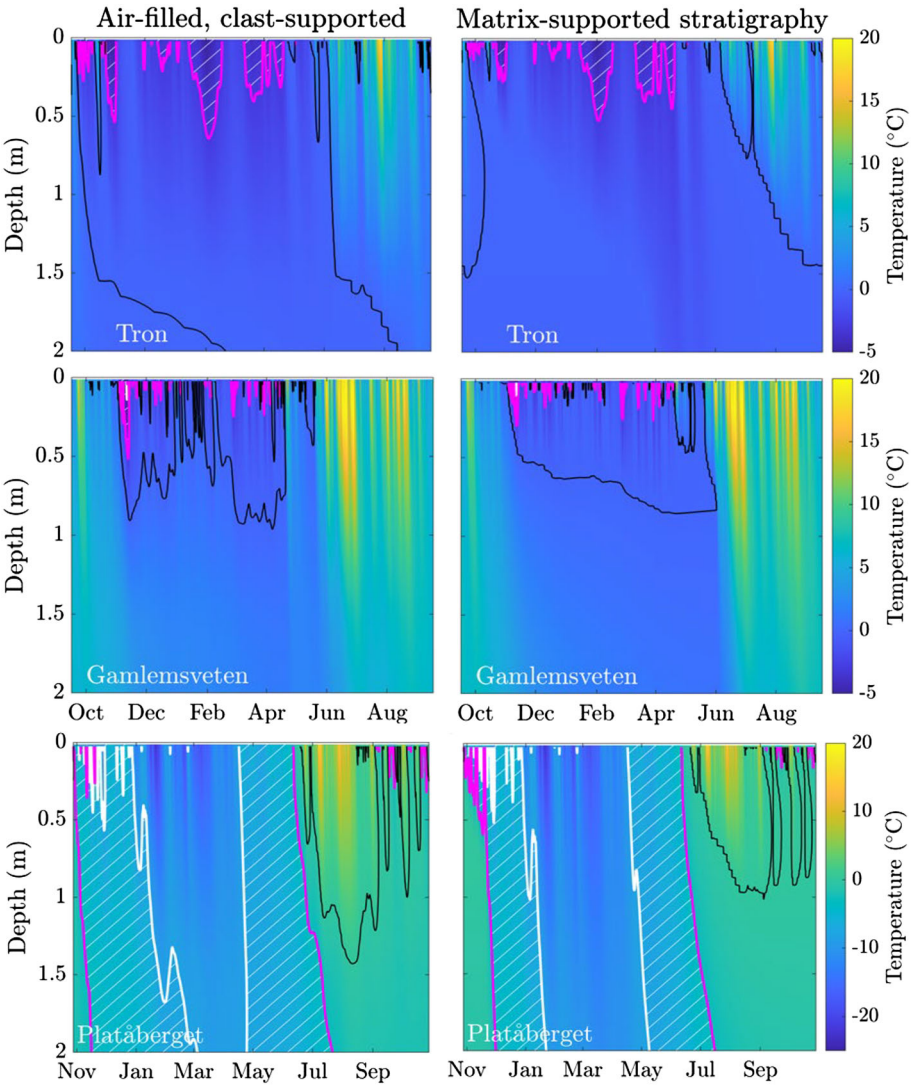

FIGURE 11 Temperature field below logger site 21 at Tron blockfield, logger 20 at Gamlemsveten blockfield and logger 7 at Platåberget blockfield, modelled for air-filled, clast-supported stratigraphy and matrix-supported stratigraphy. Note the different temperature ranges and shifted time axes. Black line shows 0°C, magenta line the −3°C curtain and white line the −8°C isotherm. The hatched areas indicate the frost-cracking window (FCW). [Color figure can be viewed at wileyonlinelibrary.com]

compared to only 1.5 m in the matrix-supported stratigraphy realization, while the − 3°C isoline enters only to a depth of 0.5–0.6 m for short periods during season 2018/2019 for both stratigraphy cases. Here the depth difference is not as pronounced. For both scenarios, permafrost would form and there is an active layer of 1.5–2.5 m depth. At Gamlemsveten blockfield the seasonal freezing penetrated about 1 m (air-filled, clast-supported) to 0.75 m (matrix-supported) deep and from November until end of May we see repeated crossing of the −3°C isotherm line. In the air-filled clast-supported stratigraphy, these pulses reach a maximum depth of 0.5 m, while in the matrix-supported stratigraphy they reach a depth of around 0.25 m.

At the Platåberget site we model an active layer of 0.9–1.4 m, depending on the stratigraphy.

In general, ground temperatures in the air-filled, clast-supported stratigraphy respond more immediately to changes in air or surface temperatures, while in the matrix-supported stratigraphy ground temperature changes are buffered at depth.

In Figure 12, we show the FCI calculated for one logger of each blockfield site for both stratigraphies, to show the impact of ground material on the FCI during the yearly cycle. At the Tron blockfield the frost cracking occurs deeper in the air-filled, clast-supported stratigraphy (to 0.65 m deep) than in the matrix-supported stratigraphy, but is 100–1000 times more intense in the air-filled, clast-supported stratigraphy, especially from October to March. After March, most soil water is frozen and the FCI values are very low, and about the same for each stratigraphy.

At Gamlemsveten frost cracking again occurs deeper in the air-filled, clast-supported stratigraphy, with FCI values between 0.1 and 1 K. In the matrix-supported stratigraphy, frost cracking occurs shallower (only to 0.3 m depth), but FCI ranges between 5 and 100 K throughout the winter season. In both stratigraphies we see repeated 'FCI spells' penetrating the ground throughout winter and spring.

At Platåberget the difference in FCI is most distinct, showing values below 0.1 K for the air-filled, clast-supported stratigraphy as compared to FCI between 10 and 100 K for the matrix-supported stratigraphy. After the active layer is completely frozen at the end of November, there is no frost-cracking activity at this field site until the next fall season. Here, the depth of FCI is comparable for both stratigraphies and reaches around 0.6 m during the fall cold spell.

At all sites, we see most intense frost cracking at the beginning of winter, before or during snow cover establishment and before the active layer is completely frozen. This is when there is still water available in deeper layers and steep temperature gradients can occur. Additional, but less intense pulses of frost cracking occur in spring during thaw and melt and repeated freezing events. In the maritime climate of Gamlemsveten, water becomes available multiple times

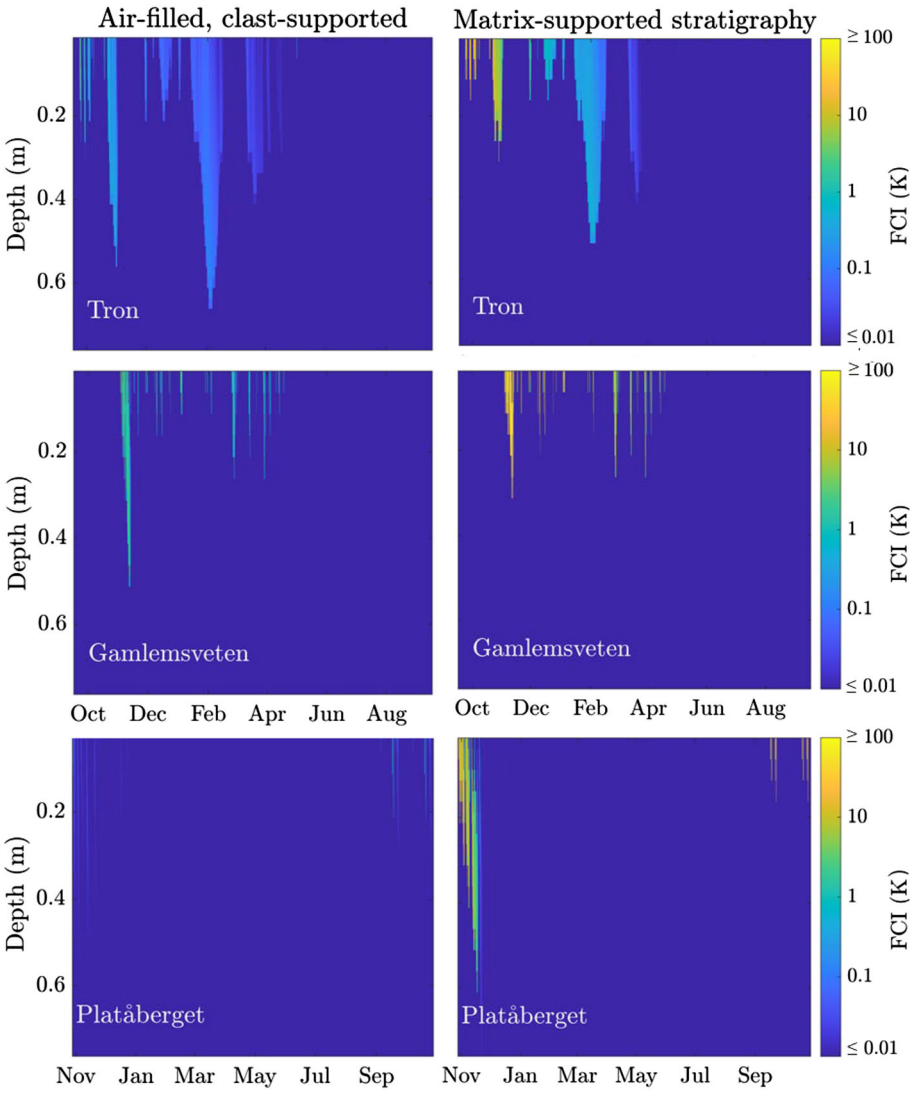

FIGURE 12 Simulated frost-cracking intensity (FCI) (K) for one logger at each blockfield site and two different stratigraphies. Note the logarithmic scale for FCI in K, the shifted observation period between Platåberget and the other two sites, and the cropped depth in comparison to Figure 11. [Color figure can be viewed at wileyonlinelibrary.com]

during the winter season, concurrent with temperature drops into the FCW. About 95% of the frost cracking at Gamlemsveten occurs above a depth of 0.35–0.4 m, depending on the stratigraphy.

Finally, we compute the annual average frost cracking intensity $\overline{FCI}$ (Andersen et al., 2015)—that is, the depth-integrated and time-averaged or cumulative FCI, shown in Figure 13, which provides a single value for each logger site, characterizing the intensity of frost cracking at each blockfield site for the two different stratigraphies.

At each blockfield site, the matrix-supported stratigraphy yielded much higher cumulative FCI (10–100 times more). This large difference was most pronounced at the Platåberget blockfield site, while at Gamlemsveten and Tron the difference was lower (around a factor of 10).

Especially at Tron and Gamlemsveten, the annual average FCI displays strong spatial variability within the sites, at least partly driven by the time spent in the frost cracking window (Section 4.3). About a third of the loggers, for both stratigraphies, experienced no or extremely low FCI and thus appeared in the zero-bin of the histograms, while there is no logger in the zero-bin for the $\overline{FCI}$ at Platåberget blockfield.

5 | DISCUSSION

5.1 | Model uncertainties

In this study we employ a purely heat-conduction-based model, driven by measurements of ground surface temperatures, to simulate depth-resolved ground temperature profiles. The model does not take advective mechanisms like water percolation and air flow into account, which can be important factors for ground temperatures in blocky terrain. However, Gruber and Hoelze (2008) showed that a purely heat-conduction-based approach can reproduce the negative temperature anomaly observed for blockfields.

In the model, the sum of water and ice content of each cell is assumed constant, so that seasonally varying ice tables as, for example, presented in Sawada (2003) are not accounted for. In the natural environment the water content of a 'grid cell' responds to precipitation, snow melt, evaporation and drainage. However, as the water holding capacity of openwork blockfields is limited, these changes are expected to be small for the air-filled, clast-supported stratigraphy, while larger changes can potentially occur for the matrix-supported stratigraphy. While more sophisticated models such as GEOTOP2.0 (Endrizzi et al., 2014) and CryoGrid3 (Zweigel et al., 2021) may improve simulations of ice and water balance in the blockfields, our simple approach driven by measurements can capture key factors governing frost cracking, such as ground surface temperature driven by local climate and snow cover, as well as differences in the ground stratigraphy.

The selected stratigraphies for this study are idealized stratigraphies constructed from qualitative observation at the three study sites where both clast-supported blockfield forms with air-filled voids and matrix-supported blockfield forms exist. Simulated ground temperature fields and FCI react very sensitively to the different stratigraphic configurations, resulting in differences of one to two orders of magnitude higher in annual average frost cracking intensity.

This suggests that the stratigraphic type of the blockfield is a key control for the overall FCI despite uncertainties in the stratigraphic parameters, such as depth of the blocky layer, porosity and water content.

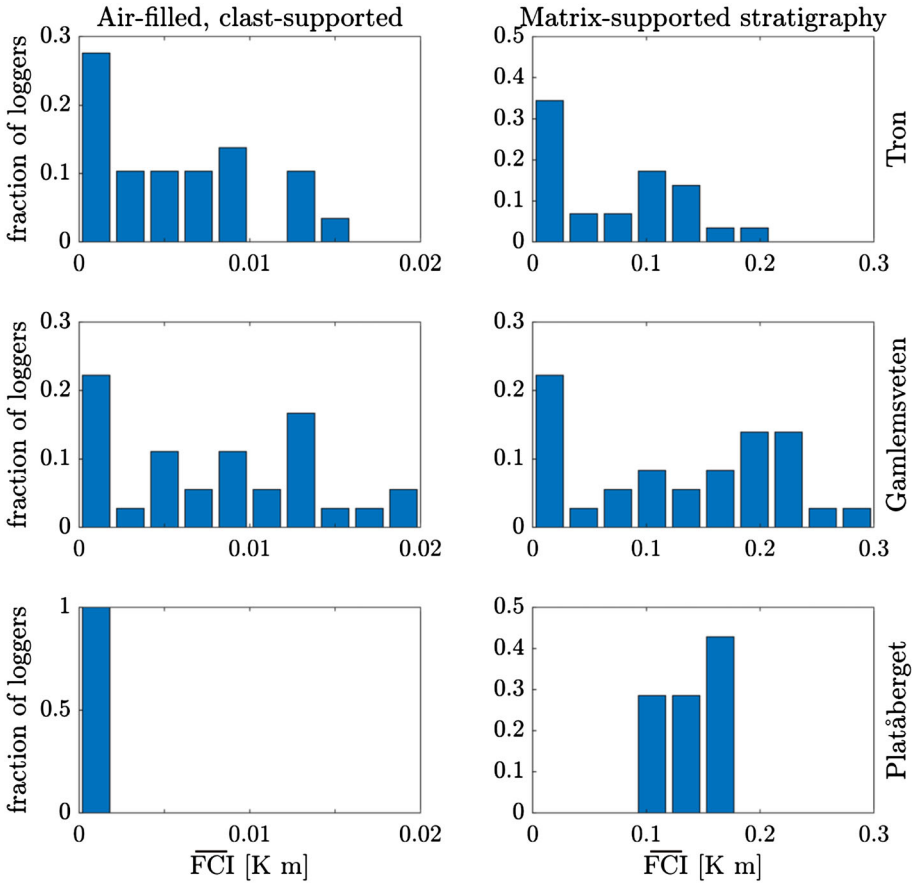

FIGURE 13 Simulated annual average frost cracking intensity $\overline{FCI}$ (K m) (depth-integrated and time-averaged) for all loggers and both stratigraphies at the three field sites. [Color figure can be viewed at wileyonlinelibrary.com]

5.2 | Factors influencing FCI

Our study design allows us to explore the effect of both climate and ground stratigraphy on FCI. The three field sites were chosen with the goal of investigating strongly different climate settings, ranging from a maritime site with no permafrost (Gamlemsveten) to a high Arctic site with low precipitation and cold permafrost (Platåberget). This provides us with a range of around 10°C in mean annual air temperature (Table 1). For all sites, the influence of the stratigraphy is investigated by simulating two stratigraphic types—that is, a clast-supported stratigraphy with air-filled pores, and a matrix-supported stratigraphy with pores filled with fines.

The coldest blockfield site at Platåberget features cold permafrost, with an estimated permafrost table at about 0.8–1.5 m depth (Figure 11) and with annual average ground temperatures between −4 and −6°C. The FCI for the active layer were extremely low, between 0.0001 and 0.001 K, depending on stratigraphy and time of the freezing season. This shows that even in a permafrost setting frost cracking is possible, but at comparatively low intensities. This suggests low frost-cracking activity for blockfields in Arctic areas, even in maritime settings.

In contrast, the Gamlemsveten blockfield site features high FCI, with no permafrost and ground temperatures above and below 0°C, with few very cold weather events. This provides the blockfield with enough water available for frost cracking during the freezing season. This maritime site in southern Norway has the highest FCI values. The blockfield also features the largest amount of vegetation and fine sediment. This is in accordance with findings from Savi et al. (2015), who state that highest frost-cracking activity in the Alps is associated with positive MAATs and temperatures around 0°C.

With a mean air temperature of −2.7°C (Table 1) and thick winter snow cover, permafrost at the Tron blockfield is likely discontinuous with simulations showing permafrost at some logger sites and no permafrost at others. Here, FCI are strongly variable in space, but are on average only slightly lower than at the warmer permafrost-free Gamlemsveten site.

Our results suggest that permafrost in blockfields, or rather the climatic conditions favouring permafrost presence, is likely to be an inhibiting factor for effective frost cracking. In general, very low to zero frost cracking occurred in settings with low water availability, as well as too warm and too low temperatures. Water availability is again connected to stratigraphy and the ground thermal regime of the different blockfields (see also the discussion in Ballantyne, 2010). In stratigraphies with a high fraction of fines (silt, sand, clay, gravel), we modelled the highest FCI, assuming surface and ground temperatures were in the frost-cracking window. For air-filled, clast-supported stratigraphies the lowest FCI were modelled for all sites.

We conclude that the occurrence of the highest FCI is not connected to one factor only but depends on an intricate interplay of several factors. High FCI are yielded by (1) air temperatures that are cycling around 0°C and are also regularly reaching the FCW throughout winter; (2) a (wet) snow cover that is 'on' and 'off' throughout the winter season, possibly with rain events in between snow cover periods; (3) no permafrost or very warm permafrost with deep active layers; (4) a matrix-supported stratigraphy with a high fraction of fines (sand, silt, clay, gravel).

Vice versa, we can summarize the lowest FCI for conditions of (1) warm (not reaching the FCW) or very cold air temperatures; (2) stable, (thick) and cold snow cover in winter, as well as early onset of snow cover before colder air temperatures occur; (3) cold permafrost, thin active layer, or no permafrost; (4) a clast-supported stratigraphy with air-filled pores and no fines.

5.3 | Implications for frost cracking since the last deglaciation

Our near-surface ground temperature and snow measurements are a snapshot in time of only 1 year. Compared to the climate normal 1961–1990, the study period had a deviation of mean air temperature of +2.0°C and 104% of mean precipitation (Table 1). In the area of the Gamlemsveten site, the temperature deviation from the normal period was +1.0°C during the study period and mean precipitation was 140% (Table 1). Temperatures increased strongly at Svalbard in the Longyearbyen area, with mean temperatures during the study period +3.7°C warmer than for the normal period. Precipitation was around 120% of normal during the study period (Table 1).

In conclusion, the study period had warmer air temperatures than the climate normal, corresponding to approximately 1–2°C warmer conditions for Tron and Gamlemsveten than during most of the Holocene (Figure 14). It is likely that the temperatures are in a similar range as during the Holocene thermal maximum. For Platåberget an even stronger warming was recorded, so that the temperatures during the Holocene were likely lower than during the study period. As the three field sites span a range of around 10°C in air temperature, we can use space-for-time substitution to infer estimates for frost cracking after deglaciation and during the Holocene. Figure 14 shows a temperature reconstruction for the Scandinavian landmass (Alley et al., 1995; Lilleøren et al., 2012), which is likely representative for the Tron and Gamlemsveten sites. In addition, the temperature reconstruction from the GISP2 ice core is shown (Alley et al., 1995), which may be more representative for the Platåberget site.

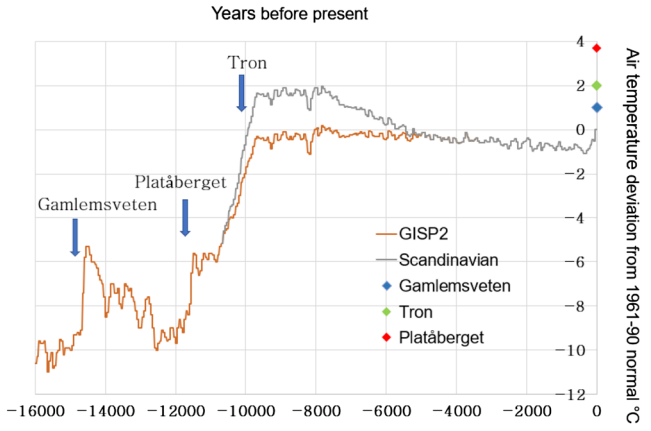

FIGURE 14 GISP2-Greenland ice sheet ice core data interpreted temperature deviation from the 1961–90 normal (Alley et al., 1995) in orange and the reconstruction of Holocene temperature deviation for the Scandinavian area (Lilleøren et al., 2012) in grey. Blue, green and red diamonds: air temperature deviations for field sites Tron, Gamlemsveten and Platåberget, respectively (from normal period 1961–90, Table 1). Blue arrows indicate deglaciation at each of the three field sites. [Color figure can be viewed at wileyonlinelibrary.com]

Our results suggest that present-day frost cracking is relatively similar for the climate conditions at Tron and Gamlemsveten sites, while being significantly smaller for the colder climate on Platåberget. Since deglaciation, the Platåberget site must have largely experienced colder climates compared to the study period, which suggests permafrost conditions and low FCI throughout the entire period, in a similar range or possibly even lower than during the study period.

The Tron site deglaciated in the early Holocene. While the FCI values during the study period are a good indication for frost cracking values during the Holocene thermal maximum, FCI may have been lower at the Tron blockfield site during the colder parts of the Holocene—possibly more comparable to the Platåberget site during the study period. In these periods, permafrost was likely more widespread at Tron, which supports the assumption of overall lower frost cracking.

The Gamlemsveten blockfield deglaciated around 15 ka and thus experienced temperature conditions 6–10°C colder than the study period until around 11 ka. Space-for-time substitution suggests that the site may have experienced permafrost conditions comparable to the Platåberget site during this period, with comparatively low FCI. During the Holocene thermal maximum, permafrost must have disappeared, in conjunction with frost cracking intensifying to values similar to the study period. During the colder parts of the Holocene, temperature conditions likely were still warmer than at the Tron site today, which suggests persistently permafrost-free conditions, except for possibly cold periods like the Little Ice Age (LIA). As Tron and Gamlemsveten feature similar FCI, the results of our study may adequately represent the overall frost cracking intensity during the Holocene at Gamlemsveten.

5.4 | Implications for blockfield development

Our study can provide constraints on the long-term evolution of blockfields. The first hypothesis is that blockfields formed before or during the Quaternary and persisted either below a cold-based ice cover or on ice-free nunataks which prevented them from being eroded (Rea et al., 1996). Assuming that blockfields were indeed stable under cold-based ice (Kleman & Glasser, 2007), our results can shed light on the blockfield evolution and stability during the ice-free periods (interglacials, interstadials and potentially nunatak phases). For the air-filled, clast-supported stratigraphy, the simulated annual average frost cracking intensity was one to two orders of magnitude lower than for the matrix-supported stratigraphy. This suggests that, in the absence of fines, blockfields are comparatively resistant to frost cracking and thus represent a highly stable landform, especially in a very cold climate with permafrost conditions which further reduce frost cracking. If one assumes that FCI is proportional to the weathering rate (Egholm et al., 2015), a difference of factor 10 in the annual average frost cracking intensity would suggest that a clast in a blockfield with air-filled voids persists 10 times longer than a clast surrounded by a matrix of fine sediments. The former could therefore require 10 interglacial periods to experience the same intensity of frost weathering as the latter in a single interglacial. Egholm et al. (2015) used a proportionality coefficient of $10^{-3}\,K^{-1}\,a^{-1}$ between FCI and weathering rate which would yield column-averaged rates of 1 m/10 ka for the matrix-supported settings of all blockfield sites (using a typical value for $\overline{FCI} = 0.1$ K m, Figure 13), 1 m/100 ka for the clast-supported cases in Tron and Gamlemsveten (for $\overline{FCI} = 0.01$ K m, Figure 13), as well as 1 m/1 Ma for the clast-supported stratigraphy on Platåberget (for $\overline{FCI} = 0.001$ K m, Figure 13). Although these values are essentially unconstrained, the comparative stability and longevity of existing blockfields is certainly consistent with the first hypothesis.

According to the second hypothesis, blockfields formed only after the last deglaciation, either emerging from glacially scoured bedrock through weathering, or by frost-induced sorting of clast-rich till. Our results suggest that clasts embedded in fine sediments would be subject to comparatively intense frost cracking and thus fast disintegration of blocks. A blockfield with air-filled voids can only persist if frost heave of clasts from deeper layers exceeds the frost-induced breakdown of clasts at the surface. Under this condition, blocks would eventually accumulate at the surface and thus produce a more long-term stable, clast-supported blockfield with reduced FCI. This process could be supported by the removal of fine material through wind or surface wash (Ballantyne, 2010). However, frost heave is restricted to clasts in the active or seasonal frost layer, which limits the supply of available clasts on plateaus. The formation of blocks from a bedrock surface can be facilitated by fractures caused by stresses of an overlying ice sheet and pressure release during deglaciation (Ballantyne, 2010). The fractures are extended by frost cracking or chemical weathering until eventually blocks and thus a shallow blockfield are produced, which would again be comparatively resistant to frost cracking (see above). To produce a thicker weathering mantle, a continued production of blocks from the buried bedrock surface is required. Under the present-day climate conditions of the study sites, our results suggest that frost cracking is widely limited to the uppermost 0.5 m. Unless the sites have experienced climate conditions which allowed for deeper frost cracking, the production of blocks from the bedrock would have to be facilitated by chemical weathering during permafrost-free conditions.

Each of the investigated blockfield sites has a different glaciation history, and landforms and sediment properties observed at or near the sites may provide insight into their development after deglaciation. Platåberget has signs of till material and old melt-water channels, but also blocky material and blockfield layering in other places. We here suggest a polygenetic evolution of the blockfield, which may have been influenced by light glacial erosion during the early Weichselian or during the Saalian but was below minimally erosive ice after that. Fluvial sediment and signs of erosion (fluvially rounded rocks, traces of melt-water channels) indicate that this plateau was the main hydrological track of deglaciation for a glacier until those glaciers retreated to another watershed. The areas with air-filled, clast-supported stratigraphy might be very stable, while the till and fluvial sediment areas experience more intense frost cracking. This blockfield cannot have formed during the Holocene time only.

Tron might be the only 'classic' blockfield with no erratics or till present at the summit, showing clast-supported stratigraphy with sorting and heave processes visible at the surface, and some tors. Due to its location far inland and at high elevation, we suggest that Tron summit was often covered by ice during the Quaternary and that the blockfield formed (and preserved) bit by bit throughout during the interstadials. It is possible that this blockfield could have experienced glacial (warm-based) erosion during the early glaciations of the Quaternary and later became a cold-based region of the ice sheets (Egholm et al., 2017).

Gamlemsveten blockfield has in certain areas a very thick fine sediment layer with sand, silt and clay developed below a layer of larger clasts. It appears to have a long history of ice-free periods during the last glaciation and low erosion rates (Sollid & Sørbel, 1979). While the high FCI values suggest strong frost weathering and thus a young age, the findings of clay minerals below the blocky layer (Roaldset et al., 1982) could be an indication of deep weathering and at the same time a protection from erosion or low erosion rates during the Quaternary.

Although the link between FCI and erosion rates is not fully clear, this study could be an indication that blockfield erosion rates can be very low in a cold and dry climate. First, a low amount of fine material is produced at low FCI and because the larger blocks at plateaus or low-angle slopes are only moved by frost heave on top of the fine material layer (in an example by Berthling et al., 2001, ploughing boulders moved up to 10 mm horizontally per year through gelifluction). Secondly, it has been shown that boulder-armoured slopes are efficiently protected from erosion in comparison to unconsolidated fine sediment, soil and bare bedrock surfaces (Granger et al., 2001). Erosion rates possibly increase when the blockfield becomes unstable; that is, more and more fines are produced and delivery of blocks from the bedrock interface stops; thus, the climate becomes warmer and more humid at the site. Then, with more fines available, the surface is more susceptible to fluvial erosion (surface wash from rain). In the case of rapid vegetation succession, erosion rates might decrease again. Although lateral movement rates cannot be constrained by the study, downslope fluxes are likely an important part of the 'block-mass balance' of the site.

The results of this study cannot conclusively prove or disprove either of the two hypotheses, but they provide important constraints on the processes involved in the formation and preservation of the blockfield landform which can enable and support future work. In particular, we need to establish quantitative constraints on frost heave of clasts within sediments and erosion rates for blockfields under different climatic conditions and different stratigraphies (which can also improve interpretation of cosmogenic nuclide dating for blockfields). Furthermore, it would be desirable to better constrain the proportionality coefficient between FCI and weathering rates (Egholm et al., 2015). Developing such relationships for blockfields would make it possible to simulate their climate-driven evolution with the periglacial landscape evolution model by Andersen et al. (2015) and Egholm et al. (2015). Such a scheme could eventually simulate key processes for blockfield development, such as the production of blocks at the bedrock interface, heave of blocks within a sediment matrix, production of sediments due to frost weathering, as well as lateral transport due to frost creep (Andersen et al., 2015) and water-induced movement of fine sediments. With such a model, the different hypotheses of blockfield survival, as well as deterioration pathways and development of a soil mantle, could be directly evaluated for different field sites to achieve a better understanding of the life cycle and lifespan of the blockfield landform.

6 | CONCLUSIONS

We investigated FCI in three different blockfields in Scandinavia and Svalbard through a modelling approach that calculates FCI from measured near-surface temperatures, temperature gradients in the ground column and water availability. These FCI provide insight into frost weathering and thus the stability of the blockfield landform in different environments.

1. Frost cracking in the blockfields never occurred deeper than about 0.7 m depth, while most intense frost cracking activity is limited to the uppermost 0.35–0.4 m. In the case of a blockfield with large boulders and blocks and large spaces in between (no sediment infill) in the upper layer, which reaches a depth of 1–2 m, frost cracking occurs to 1.5 m depth, depending on the time point of snow infill of the hollows.
2. In the Gamlemsveten blockfield, the FCI were the highest of all sites. The relatively warm winters and hence temperatures fluctuating above 0°C and in and out of the FCW were the main driver of high FCI. Additionally, the repeated freezing, snow cover onset and melting of the snow cover plus winter rain events provided repeated moisture sources for new frost cracking during the winter season.
3. Lowest FCI were modelled for Platåberget on Svalbard, where it was often too cold for frost-cracking to occur. At the same time, the cold permafrost ground and shallow active layer inhibited frost cracking by reducing water availability during winter.
4. Water availability and stratigraphy strongly affect FCI. At all sites, the FCI sensitively responded to increases or decreases in water availability—much more compared to parameters like temperatures or porosity.
5. The stratigraphy that favoured highest FCI was clasts (blocks and boulders) sitting in a matrix of sand, silt and gravel (matrix-supported stratigraphy). This is because the finer material can hold higher amounts of water than an open-work blockfield. We find this type of stratigraphy in areas of sorted ground, like sorted circles and polygonal structures within blockfields. In these settings, we can also observe a stronger influence of frost sorting across the ground column. Outside of blockfields but possibly in the same climate setting, we find this stratigraphy for till deposits.

Our results suggest that plateau blockfields could be a stable landform with low erosion rates in a certain climate setting. This study is a step towards a better understanding towards periglacial landscape evolution and its conceptualization in numerical models.

AUTHOR CONTRIBUTIONS

The study was planned by MP and contributions from the supervisors. MP carried out the data collection and assessment and wrote the manuscript. The CryoGrid code was provided by SW and further developed by MP. All authors reviewed the study results and revised the manuscript. FCN, BE, and OF functioned as supervisors. MP secured funding for fieldwork on Svalbard through an Arctic Field Grant of the Research Council of Norway.

ACKNOWLEDGEMENTS

We gratefully acknowledge the financial support from the Department of Geography at the Norwegian University of Science and Technology and the Arctic Field Grant (Research Council of Norway, grant no. ES676559). We also gratefully acknowledge field work assistance by Radmil Popovic, Henriette Linge, Susanne Hegstad, Emil Krokan, Jogeir Søvik, Ullrich Neumann, Kolibri Geoservices, Marte Westad, Emiliano Santin, Rémi Dallmayr, Mari Hurrød Larsen, Leo Decaux, Sigurrós Arnardóttir, Jacek Jania, Thibault Desjonquères, and Craig Hammock.

CONFLICT OF INTEREST STATEMENT

The authors have no conflict of interest to declare.

DATA AVAILABILITY STATEMENT

The data that support the findings of this study are openly available at https://doi.org/10.5281/zenodo.7026148.

ORCID

Maria Peter https://orcid.org/0000-0001-6986-4315
Jane Lund Andersen https://orcid.org/0000-0003-2829-6352
Francis Chantel Nixon https://orcid.org/0000-0002-6113-100X

REFERENCES

Alley, R.B., Gow, A.J., Johnsen, S.J., Kipfstuhl, J., Meese, D.A. & Thorsteinsson, T. (1995) Comparison of deep ice cores. *Nature*, 373(6513), 393–394. Available from: https://doi.org/10.1038/373393b0

Andersen, J.L., Egholm, D.L., Knudsen, M.F., Jansen, J.D. & Nielsen, S.B. (2015) The periglacial engine of mountain erosion – Part 1: Rates of frost cracking and frost creep. *Earth Surface Dynamics*, 3(4), 447–462. Available from: https://doi.org/10.5194/esurf-3-447-2015

Andersen, J.L., Egholm, D.L., Knudsen, M.F., Linge, H., Jansen, J.D., Goodfellow, B.W., et al. (2018) Pleistocene evolution of a Scandinavian plateau landscape. *Journal of Geophysical Research - Earth Surface*, 123(12), 3370–3387. Available from: https://doi.org/10.1029/2018JF004670

Anderson, R.S. (1998) Near-surface thermal profiles in Alpine bedrock: Implications for the frost weathering of rock. *Arctic and Alpine Research*, 30(4), 362–372. Available from: https://doi.org/10.2307/1552008

Anderson, R.S. (2002) Modeling the tor-dotted crests, bedrock edges, and parabolic profiles of high alpine surfaces of the Wind River range, Wyoming. *Geomorphology*, 46(1–2), 35–58. Available from: https://doi.org/10.1016/S0169-555X(02)00053-3

Ballantyne, C.K. (1998) Age and significance of mountain-top detritus. *Permafrost and Periglacial Processes*, 9(4), 327–345. Available from: https://doi.org/10.1002/(SICI)1099-1530(199810/12)9:4<327::AID-PPP298>3.0.CO;2-9

Ballantyne, C.K. (2010) A general model of autochthonous Blockfield evolution. *Permafrost and Periglacial Processes*, 21(4), 289–300. Available from: https://doi.org/10.1002/ppp.700

Berthling, I., Eiken, T., Madsen, H. & Sollid, J.L. (2001) Downslope displacement rates of ploughing boulders in a mid-alpine environment: Finse, southern Norway. *Geografiska Annaler*, 83(3), 103–116. Available from: https://doi.org/10.1111/j.0435-3676.2001.00147.x

Berthling, I. & Etzelmüller, B. (2011) The concept of cryo-conditioning in landscape evolution. *Quaternary Research*, 75(2), 378–384. Available from: https://doi.org/10.1016/j.yqres.2010.12.011

Biskaborn, B.K., Smith, S.L., Noetzli, J., Matthes, H., Vieira, G., Streletskiy, D.A., et al. (2019) Permafrost is warming at a global scale. *Nature Communications*, 10(1), 1–11. Available from: https://doi.org/10.1038/s41467-018-08240-4

Briner, J.P., Miller, G.H., Davis, P.T. & Finkel, R.C. (2006) Cosmogenic radionuclides from fiord landscapes support differential erosion by overriding ice sheets. *Geological Society of America Bulletin*, 118(3–4), 406–420. Available from: https://doi.org/10.1130/B25716.1

Cosenza, P., Guerin, R., Tabbagh, A. (2003) Relationship between thermal conductivity and water content of soils using numerical modeling. *European Journal of Soil Science*, 54, 581–588.

Dall'Amico, M., Endrizzi, S., Gruber, S. & Rigon, R.J.T.C. (2011) A robust and energy-conserving model of freezing variably-saturated soil. *The Cryosphere*, 5(2), 469–484. Available from: https://doi.org/10.5194/tc-5-469-2011

Egholm, D., Jansen, J., Brædstrup, C., Pedersen, V.K., Andersen, J.L., Ugelvik, S.V., et al. (2017) Formation of plateau landscapes on glaciated continental margins. *Nature Geoscience*, 10(8), 592–597. Available from: https://doi.org/10.1038/ngeo2980

Egholm, D.L., Andersen, J.L., Knudsen, M.F., Jansen, J.D. & Nielsen, S.B. (2015) The periglacial engine of mountain erosion – Part 2: Modelling large-scale landscape evolution. *Earth Surface Dynamics*, 3(4), 463–482. Available from: https://doi.org/10.5194/esurf-3-463-2015

Endrizzi, S., Gruber, S., Dall'Amico, M. & Rigon, R. (2014) GEOtop 2.0: Simulating the combined energy and water balance at and below the land surface accounting for soil freezing, snow cover and terrain effects. *Geoscientific Model Development*, 7(6), 2831–2857. Available from: https://doi.org/10.5194/gmd-7-2831-2014

Fjellanger, J., Sørbel, L., Linge, H., Brook, E.J., Raisbeck, G.M. & Yiou, F. (2006) Glacial survival of blockfields on the Varanger peninsula, northern Norway. *Geomorphology*, 82(3–4), 255–272. Available from: https://doi.org/10.1016/j.geomorph.2006.05.007

Fraser, J.K. (1959) Freeze-thaw frequencies and mechanical weathering in Canada. *Arctic*, 12(1), 40–53. Available from: https://doi.org/10.14430/arctic3712

Geiger, R. (1954) Klassifikation der Klimate nach W. Köppen. In: *Landolt-Börnstein. Zahlenwerte und Funktionen aus Physik, Chemie, Astronomie, Geophysik und Technik, alte Serie*, Vol. 3. Berlin: Ch., Springer, pp. 603–607.

Goehring, B.M., Brook, E.J., Linge, H., Raisbeck, G.M. & Yiou, F. (2008) Beryllium-10 exposure ages of erratic boulders in southern Norway and implications for the history of the Fennoscandian ice sheet. *Quaternary Science Reviews*, 27(3–4), 320–336. Available from: https://doi.org/10.1016/j.quascirev.2007.11.004

Goodfellow, B.W. (2012) A granulometry and secondary mineral fingerprint of chemical weathering in periglacial landscapes and its application to blockfield origins. *Quaternary Science Reviews*, 57, 121–135. Available from: https://doi.org/10.1016/j.quascirev.2012.09.023

Goodfellow, B.W., Fredin, O., Derron, M.-H. & Stroeven, A.P. (2009) Weathering processes and quaternary origin of an alpine blockfield in Arctic Sweden. *Boreas*, 38(2), 379–398. Available from: https://doi.org/10.1111/j.1502-3885.2008.00061.x

Goodfellow, B.W., Stroeven, A.P., Fabel, D., Fredin, O., Derron, M.H., Bintanja, R., et al. (2014) Arctic–alpine blockfields in the northern Swedish Scandes: Late Quaternary–not Neogene. *Earth Surface Dynamics*, 2(2), 383–401. Available from: https://doi.org/10.5194/esurf-2-383-2014

Granger, D.E., Riebe, C.S., Kirchner, J.W. & Finkel, R.C. (2001) Modulation of erosion on steep granitic slopes by boulder armoring, as revealed by cosmogenic 26Al and 10Be. *Earth and Planetary Science Letters*, 186(2), 269–281. Available from: https://doi.org/10.1016/S0012-821X(01)00236-9

Gruber, S., & Hoelze, M. (2008) The cooling effect of coarse blocks revisited: a modeling study of a purely conductive mechanism. In: *9th International Conference on Permafrost*, Fairbanks, Alaska, 29 June 2008–3 July 2008, 557–561.

Hales, T.C. & Roering, J.J. (2007) Climatic controls on frost cracking and implications for the evolution of bedrock landscapes. *Journal of Geophysical Research*, 112(F2), F02033. Available from: https://doi.org/10.1029/2006JF000616

Hall, K., Thorn, C., Matsuoka, N. & Prick, A. (2002) Weathering in cold regions: Some thoughts and perspectives. *Progress in Physical Geography*, 26(4), 577–603. Available from: https://doi.org/10.1191/0309133302pp353ra

Hallet, B., Walder, J.S. & Stubbs, C.W. (1991) Weathering by segregation ice growth in microcracks at sustained sub-zero temperatures: Verification from an experimental study using acoustic emissions. *Permafrost and Periglacial Processes*, 2(4), 283–300. Available from: https://doi.org/10.1002/ppp.3430020404

Hughes, A.L.C., Gyllencreutz, R., Lohne, Ø.S., Mangerud, J. & Svendsen, J.I. (2016) The last Eurasian ice sheets – A chronological database and time-slice reconstruction, DATED-1. *Boreas*, 45(1), 1–45. Available from: https://doi.org/10.1111/bor.12142

Isaksen, K., Holmlund, P., Sollid, J.L. & Harris, C. (2001) Three deep alpine-permafrost boreholes in Svalbard and Scandinavia. *Permafrost and Periglacial Processes*, 12(1), 13–25. Available from: https://doi.org/10.1002/ppp.380

Jansen, J.D., Knudsen, M.F., Andersen, J.L., Heyman, J. & Egholm, D.L. (2019) Erosion rates in Fennoscandia during the past million years. *Quaternary Science Reviews*, 207, 37–48. Available from: https://doi.org/10.1016/j.quascirev.2019.01.010

Jansson, A., Tveito, O.E., Pirinen, P., & Scharling, M. (2007) NORDGRID: a preliminary investigation on the potential for creation of a joint Nordic gridded climate dataset. Norwegian Meteorological Institute, Oslo, Norway, Climate Report No. 03.

Juliussen, H. & Humlum, O. (2008) Thermal regime of openwork block fields on the mountains Elgåhogna and Sølen, Central-Eastern Norway. *Permafrost and Periglacial Processes*, 19(1), 1–18. Available from: https://doi.org/10.1002/ppp.607

Kessler, M., Anderson, R. & Briner, J. (2008) Fjord insertion into continental margins driven by topographic steering of ice. *Nature Geoscience*, 1(6), 365–369. Available from: https://doi.org/10.1038/ngeo201

Kleman, J. (1994) Preservation of landforms under ice sheets and ice caps. *Geomorphology*, 9(1), 19–32, ISSN 0169-555X. Available from: https://doi.org/10.1016/0169-555X(94)90028-0

Kleman, J. & Glasser, N. (2007) The subglacial thermal organization (STO) of ice sheets. *Quaternary Science Reviews*, 25(5-6), 585–597. Available from: https://doi.org/10.1016/j.quascirev.2006.12.010

Kleman, J. & Stroeven, A.P. (1997) Preglacial surface remnants and quaternary glacial regimes in northwestern Sweden. *Geomorphology*, 19(1–2), 35–54. Available from: https://doi.org/10.1016/S0169-555X(96)00046-3

Lilleøren, K.S., Etzelmüller, B., Schuler, T.V., Gisnås, K. & Humlum, O. (2012) The relative age of mountain permafrost — Estimation of Holocene permafrost limits in Norway. *Global and Planetary Change*, 92-93, 209–223. Available from: https://doi.org/10.1016/j.gloplacha.2012.05.016

Lønne, I. (2017) Terrestrial slopes in northern high latitudes: A paradigm shift regarding sediment origin, composition, and dynamic evolution. *Geomorphology*, 276, 180–202. Available from: https://doi.org/10.1016/j.geomorph.2016.10.004

Marquette, G.C., Gray, J.T., Gosse, J.C., Courchesne, F., Stockli, L., Macpherson, G., et al. (2004) Felsenmeer persistence under non erosive ice in the Torngat and Kaumajet mountains, Quebec and Labrador, as determined by soil weathering and cosmogenic nuclide exposure dating. *Canadian Journal of Earth Sciences*, 41(1), 19–38. Available from: https://doi.org/10.1139/e03-072

Myhra, K.S., Westermann, S. & Etzelmüller, B. (2017) Modelled distribution and temporal evolution of permafrost in steep rock walls along a latitudinal transect in Norway by CryoGrid 2D. *Permafrost and Periglacial Processes*, 28(1), 172–182. Available from: https://doi.org/10.1002/ppp.1884

Myhra, K.S., Westermann, S. & Etzelmüller, B. (2019) Modeling conductive heat flow between steep rock walls and talus slopes – Thermal processes and geomorphological implications. *Frontiers in Earth Science*, 7, 192. Available from: https://doi.org/10.3389/feart.2019.00192

Nesje, A., Anda, E., Rye, N., Lien, R., Hole, P.A. & Blikra, L.H. (1987) The vertical extent of the late Weichselian ice sheet in the Nordfjord-Møre area, western Norway. *Norsk Geologisk Tidsskrift*, 67, 125–141.

Nesje, A., Dahl, S.O., Anda, E. & Rye, N. (1988) Blockfields in southern Norway: Significance for the late Weichselian ice sheet. *Norsk Geologisk Tidsskrift*, 68, 14–169.

Nesje, A., McCarroll, D. & Dahl, S.O. (1994) Degree of rock surface weathering as an indicator of ice-sheet thickness along an east-west transect across southern Norway. *Journal of Quaternary Science*, 9(4), 337–347. Available from: https://doi.org/10.1002/jqs.3390090404

Peel, M.C., Finlayson, B.L. & McMahon, T.A. (2007) Updated world map of the Köppen-Geiger climate classification. *Hydrology and Earth System Sciences*, 11(5), 1633–1644. Available from: https://doi.org/10.5194/hess-11-1633-2007

Pope, G.A., Dorn, D.I. & Dixon, J.C. (1995) A new conceptual model for understanding geographical variations in weathering. *Annals of the Association of American Geographers*, 85, 38–64.

Rae, A.C., Harrison, S., Mighall, T. & Dawson, A.G. (2004) Periglacial trimlines and nunataks of the last glacial maximum: The gap of Dunloe, Southwest Ireland. *Journal of Quaternary Science*, 19(1), 87–97. Available from: https://doi.org/10.1002/jqs.807

Rea, B.R., Whalley, W.B., Rainey, M.M. & Gordon, J.E. (1996) Blockfields, old or new? Evidence and implications from some plateaus in northern Norway. *Geomorphology*, 15(2), 109–121. Available from: https://doi.org/10.1016/0169-555X(95)00118-O

Roaldset, E., Pettersen, E., Longva, O. & Mangerud, J. (1982) Remnants of preglacial weathering in western Norway. *Norsk Geologisk Tidsskrift*, 62, 169–178.

Savi, S., Delunel, R. & Schlunegger, F. (2015) Efficiency of frost-cracking processes through space and time: An example from the eastern Italian Alps. *Geomorphology*, 232, 248–260. Available from: https://doi.org/10.1016/j.geomorph.2015.01.009

Sawada, Y. (2003) Monitoring of ground-ice formation in a block slope at Mt. Nishi-Nupukaushinupuri, Hokkaido, Japan. In *Proceedings of the 8th International Permafrost Conference*. Balkema, Lisse (pp. 1001-1005).

Skov, D.S., Andersen, J.L., Olsen, J., Jacobsen, B.H., Knudsen, M.F., Jansen, J.D., et al. (2020) Constraints from cosmogenic nuclides on the glaciation and erosion history of dove Bugt, Northeast Greenland. *GSA Bulletin*, 132(11–12), 2282–2294. Available from: https://doi.org/10.1130/B35410.1

Sollid, J.L. & Sørbel, L. (1979) Deglaciation of western Central Norway. *Boreas*, 8(2), 233–239. Available from: https://doi.org/10.1111/j.1502-3885.1979.tb00805.x

Staiger, J.K.W., Gosse, J.C., Johnson, J.V., Fastook, J., Gray, J.T., Stockli, D. F., et al. (2005) Quaternary relief generation by polythermal glacier ice. *Earth Surface Processes and Landforms*, 30, 1145–1159. Available from: https://doi.org/10.1002/esp.1267

Stroeven, A.P., Hättestrand, C., Kleman, J., Heyman, J., Fabel, D., Fredin, O., et al. (2016) Deglaciation of Fennoscandia. *Quaternary Science Reviews*, 147, 91–121. Available from: https://doi.org/10.1016/j.quascirev.2015.09.016

Strømsøe, J.R. & Paasche, Ø. (2011) Weathering patterns in high-latitude regolith. *Journal of Geophysical Research*, 116(F3), F03021. Available from: https://doi.org/10.1029/2010JF001954

Walder, J. & Hallet, B. (1985) A theoretical model of the fracture of rock during freezing. *Geological Society of America Bulletin*, 96(3), 336346. Available from: https://doi.org/10.1130/0016-7606(1985)96<336:ATMOTF>2.0.CO;2

Warren, W.P. (1979) Moraines on the northern slopes and foothills of the Macgillycuddy's Reeks, south-west Ireland. In: Schlüchter, C. (Ed.) *Moraines and Varves*. Rotterdam: Balkema, pp. 223–236.

Westermann, S., Schuler, T.V., Gisnås, K. & Etzelmüller, B. (2013) Transient thermal modeling of permafrost conditions in southern Norway. *The Cryosphere*, 7(2), 719–739. Available from: https://doi.org/10.5194/tc-7-719-2013

Zasadni, J. & Kłapyta, P. (2014) The Tatra Mountains during the last glacial maximum. *Journal of Maps*, 10(3), 440–456. Available from: https://doi.org/10.1080/17445647.2014.885854

Zweigel, R.B., Westermann, S., Nitzbon, J., Langer, M., Boike, J., Etzelmüller, B., et al. (2021) Simulating snow redistribution and its effect on ground surface temperature at a high-Arctic site on Svalbard. *Journal of Geophysical Research - Earth Surface*, 126(3), e2020JF005673.

How to cite this article: Peter, M., Andersen, J.L., Nixon, F.C., Etzelmüller, B., Westermann, S. & Fredin, O. (2023) Near-surface temperatures and potential for frost weathering in blockfields in Norway and Svalbard. *Earth Surface Processes and Landforms*, 48(5), 940–955. Available from: https://doi.org/10.1002/esp.5528